Linear Signal Processing by Acoustic Surface-Wave Transversal Filters

CARLO ATZENI AND LEONARDO MASOTTI

A Review

Abstract—**The impulse response of acoustic surface-wave (ASW) filters is determined by the configuration of an array of planar transducers tapping the acoustic signal propagated in the piezoelectric substrate. The transducer configuration is derived here by applying the general procedure used for the synthesis of linear transversal filters, which consists in time sampling the required impulse response and arranging the spacing and weights of the taps according to the time intervals and amplitudes of the impulse-response samples. The design of the tapping structure that synthesizes the impulse response of ASW transversal filters is based on a nonuniform sampling procedure, previously developed by the authors, that meets the particular requirements of ASW device operation. The features of this design procedure are presented, and several geometries of tapping transducers corresponding to impulse responses of different characteristics are discussed. The application of the procedure to the design of typical ASW filters is illustrated by the results of experimental models.**

I. Introduction

SINCE the development of the first transducers capable of launching or detecting acoustic waves propagated along the surface of a piezoelectric substrate, scientists working in the field of signal processing envisioned the potential applications of a delay line offering a new fundamental degree of freedom: the possibility of a continuous access to the traveling signal in any point of the propagation path. Signal-processing devices had previously been implemented by tapping bulk acoustic waves propagated in suitable three-dimensional structures [1]; however, the technique of tapping surface acoustic waves by transducers consisting of metal strips directly deposited on the propagation surface [2] led one to conceive the capability of achieving the same filtering functions with planar structures, whose fabrication required techniques analogous to those employed for integrated circuits, and thus appeared easy and highly reproducible.

The interest was first attracted by the possibility of implementing delay lines having dispersive characteristics; by arranging on the propagation surface a planar array of suitably spaced selective transducers, one could be able to obtain a delay variable with frequency depending only on the transducer geometry. This new technique of achieving a dispersive characteristic was first devised by Rowen [3]. Successively, a great amount of work was devoted to the implementation of acoustic surface-wave (ASW) dispersive signal processors, in particular to meet the signal-processing needs of matched filters for radar systems [4].

The further basic degree of freedom offered by ASW tapping was later pointed out in the possibility of weighting the amplitude of the detected signal simply by varying the aperture of the transducer parallel to the acoustic wavefront. Based on this property, the possibility was realized of weighting the frequency response of ASW devices by implementing arrays of transducers with suitably graded apertures [5]. Planar transducers having two-dimensional structures were so designed, consisting of arrays of parallel electrodes whose spacing along the propagation direction determined the time delay of the generated/detected signal outputs and whose aperture normal to the propagation direction determined the corresponding weights [6]. As pointed out by Squire *et al.* [7], these two degrees of freedom constitute the basic parameters for the synthesis of the transfer function of any linear filter. The synthesis of ASW filters was theoretically investigated by Tancrell and Holland [8] and by the authors [9] using different approaches. Tancrell and Holland described a model of ASW filter operation in the frequency domain. Our analysis is based on the concept that ASW filters can be considered as a particular implementation of Kallmann's transversal filters [10], and the transducer design can be derived from sampling theory in the time domain. In fact, each single electrode, detecting the electric field associated with the piezoelectric wave traveling beneath, provides a sample of the propagated signal. An array of electrodes graded in spacing and aperture thus provides a set of signal samples accordingly delayed and weighted. When an impulse, propagating along the line, passes such an array, the resulting response is a set of samples reproducing in time the spatial configuration of the array. In other words, the array configuration is a stationary replica of a time-sampled version of the desired impulse-response function.

This paper shows how planar-transducer geometries can be designed that synthesize in a sampled form the impulse response corresponding to any specified transfer function. The design procedure derives from the application to the general theory of linear transversal filters of a particular sampling procedure, previously developed by the authors [9].

II. Concept of Transversal Filter

In linear transversal filters, first described by Kallmann, the filtering function is synthesized by tapping at appropriate points the signal launched in a lossless nondispersive delay line, and weighting and summing the signal contributions from the taps (Fig. 1). The design procedure consists in sampling in the time domain the required impulse response and in arranging the positions, weights, and polarity of the taps in accordance with the time intervals, amplitudes, and sign of the impulse-response samples.

Let $h(t)$ represent the filter's impulse response and τ_i and A_i the occurrence time and the value of the ith sample, respectively. Then, the corresponding tap must be delayed by τ_i, weighed by $|A_i|$, and its polarity determined according to the sign of A_i. Assuming lightly coupled nonreflecting taps, the transversal-filter impulse response is given by the sample

Manuscript received September 28, 1972.
The authors are with the Istituto di Ricerca sulle Onde Elettromagnetiche, Consiglio Nazionale delle Ricerche, Florence, Italy.

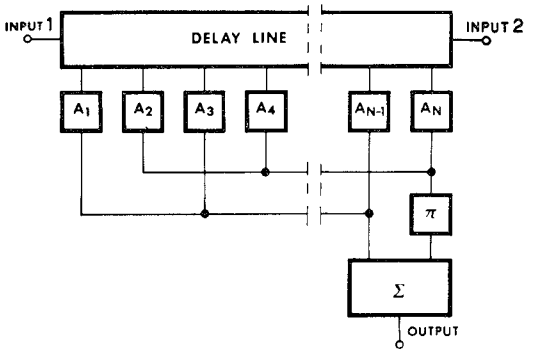

Fig. 1. Scheme of a transversal filter.

sequence

$$h_S(t) = \sum_i A_i \delta(t - \tau_i) \tag{1}$$

where δ is the Dirac impulse function. As is well known, the corresponding frequency response consists of the desired transfer function, i.e., the Fourier transform of $h(t)$, and of a number of harmonic components. Under proper conditions, the fundamental frequency response can be selected by bandpass filtering, and thus the overall impulse response of the device at the output of the cascaded bandpass filter is the required function $h(t)$.

This procedure permits, in principle, the synthesis of any linear filter. The practical implementation of such a device, however, requires a means for controlling the spacing and weighting of the tapping elements. ASW delay lines offer this capability, since, as mentioned above, continuous tapping and weighting of surface waves can be achieved by controlling the spacing and aperture, respectively, of surface-electrode transducers. The geometry of this tapping structure and the manner of inserting the required tap polarity is discussed in a following section.

III. Phase-Sampling Procedure

The design of the tapping electrode configuration of an ASW transversal filter requires the determination of a sampled form of the wanted impulse response. Since the time characteristics of the impulse-response function are known *a priori*, we have the possibility of choosing the sampling procedure most suitable for the design of a simple and efficient tapping structure. The question arises from which sampling procedure results the most convenient for the particular operation of surface-wave devices.

The first ASW filters that have been realized were dispersive devices, implemented by varying the periodicity of an array of finger-like electrodes of constant aperture according to the change of acoustic wavelength in the desired frequency range. The dispersive characteristic of such a structure was intuitively explained by considering that each frequency component was generated or detected at the position along the array where the electrode spacing was dimensioned to the corresponding wavelength; the time delays of different frequencies were so determined by the distances of the corresponding groups of electrodes [11].

The effort of framing this intuitive design criterion into the general method of transversal-filter synthesis led the authors to the development of a new procedure of sampling the filter impulse response. In order to understand the basic idea of this sampling procedure, let us consider first an impulse response having a rectangular envelope and arbitrary phase-modulation (PM) law, represented by

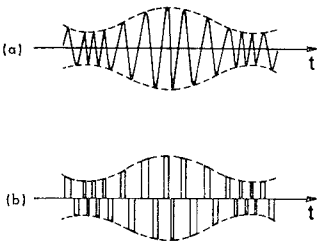

Fig. 2. Example of the phase-sampling procedure. (a) Continuous waveform. (b) Phase-sampled waveform.

$$h(t) = \cos \phi(t), \qquad |t| \leq \frac{T}{2}$$
$$= 0, \qquad \text{elsewhere.} \tag{2}$$

In general, sampling of this waveform at uniform time intervals, as suggested by the Shannon theorem, would yield samples of nonuniform amplitude, and thus the corresponding tapping electrodes of an ASW transversal filter ought to be of nonuniform aperture. This is not a desirable feature, since constancy of the electrode aperture ensures maximum energy collection and uniform illumination for all the array. Moreover, the velocity of surface elastic waves changes under the electrode metallization so that phase and amplitude distortions of the traveling wave are caused by fingers of nonuniform aperture [12].

Samples all having the same amplitude can be obtained by sampling $h(t)$ (2) in correspondence with its positive and negative peaks, i.e., *where the instantaneous phase $\phi(t)$ assumes values as multiples of π*. Since the positions of these sampling points depend on the PM law, the requirement of uniform sample amplitude leads, in general, to a nonuniform sampling interval. In the next section it will be discussed under which conditions this particular sampling procedure permits the reconstruction of the continuous waveform $h(t)$.

When the impulse response is also amplitude modulated, i.e., has the form

$$h(t) = a(t) \cos \phi(t) \tag{3}$$

where $a(t)$ is a positive envelope function, the samples determined according to the above criterion are no longer of constant amplitude; however, they have maximum amplitude[1] with respect to that obtainable using any other sampling procedure.

Finally, when the impulse response is not phase modulated, i.e.,

$$h(t) = a(t) \cos (2\pi f_0 t) \tag{3'}$$

where f_0 is a constant carrier frequency, the sampling interval becomes uniform, and the phase-sampling procedure coincides with the classical Shannon's one.

IV. Reconstruction of Phase-Sampled Waveforms

Let us consider the general waveform (3), which is both amplitude and phase modulated, and assume as sampling points the times t_n, where the instantaneous phase $\phi(t)$ is a multiple of π, i.e.,

[1] This may not be rigorously true because of the weighting effect of the envelope $a(t)$; the difference, however, is usually negligible.

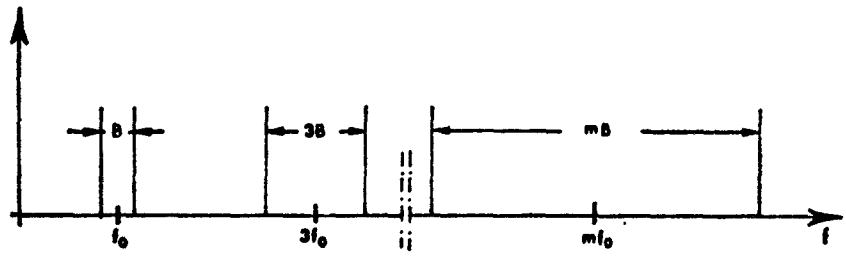

Fig. 3. Spectral band distribution of a phase-sampled waveform.

$$\phi(t) = n\pi, \qquad n = \text{integer}. \tag{4}$$

The set of the so-obtained δ-function samples can be written as

$$h_S(t) = h(t) \sum_n \delta[\phi(t) - n\pi]$$

$$= a(t) \sum_n (-1)^n \delta[\phi(t) - n\pi] \tag{5}$$

where the summation is extended to all the values of n consistent with (4). The sequence of δ-functions

$$\sum_n (-1)^n \delta[\phi(t) - n\pi] \tag{6}$$

is constructed by sampling the oscillating factor $\cos \phi(t)$ of $h(t)$ (3), and has constant periodicity *with respect to* $\phi(t)$. When considering samples having finite width (i.e., not δ-functions), which is the case of physical interest, we are therefore led to introduce, in place of (6), a train of rectangular pulses still having the periodicity of $\cos \phi(t)$, that is, having a uniform interval and width *with respect to* $\phi(t)$. The nth of such pulses has leading and trailing edges, respectively, at the times t_{n1} and t_{n2}, where

$$\phi(t) = n\pi \mp \frac{\rho}{2}, \qquad \text{with } \rho \leq \pi \tag{7}$$

and has the same sign of $\cos \phi(t_n)$.

This sequence of pulses of alternate sign, constant period 2π, and width ρ, with respect to $\phi(t)$, can be expanded into a Fourier series obtaining

$$\sum_{1\ m\ \text{odd}}^{\infty} C_m \cos [m\phi(t)] \tag{8}$$

where the zero and even harmonic terms are missing and the odd Fourier coefficients are given by

$$C_m = \frac{4}{\pi m} \sin\left(m \frac{\rho}{2}\right), \qquad m \text{ odd}. \tag{9}$$

The sampled version $h_S(t)$ of $h(t)$ thus becomes

$$h_S(t) = a(t) \sum_{1\ m\ \text{odd}}^{\infty} C_m \cos [m\phi(t)]. \tag{10}$$

An example of a phase-sampled function is shown in Fig. 2; samples result of nonuniform width in the time domain,[2] the leading/trailing edges of two adjacent samples occurring at the times where the phase $\phi(t)$ is increased by π.

The expression (10) enables one to simply evaluate the spectral distribution of the sampled waveform. In fact, the fundamental Fourier component of $h_S(t)$ coincides, apart from the amplitude factor C_1, with the continuous waveform $h(t)$, and thus its spectrum coincides with the spectrum $H(f)$ of $h(t)$. The harmonic components are waveforms of the same structure of $h(t)$, but have instantaneous phase $m\phi(t)$ modified by the factor m with respect to the phase $\phi(t)$ of $h(t)$. Their spectra can be approximately evaluated using the principle of stationary phase [14], which yields to the fundamental result that *the harmonic spectra all have the same fractional bandwidth.* In fact, we have shown [9] that the spectral amplitude $|H^m(f)|$ of the mth harmonic $h^m(t)$ is related to that $|H(f)|$ of $h(t)$ by

$$|H^m(f)| = \frac{|C_m|}{\sqrt{m}} \left| H\left(\frac{f}{m}\right) \right|. \tag{11}$$

Hence, the spectrum $H^m(f)$ at the frequency f has an amplitude proportional to that of $H(f)$ at the frequency f/m. Denoting by B the bandwidth of $h(t)$ and by f_0 the center frequency, this means that the bandwidth B^m of the mth harmonic component is $B^m = mB$ and its center frequency is $f_0{}^m = mf_0$, so that the fractional bandwidth

$$\frac{B^m}{f_0{}^m} = \frac{B}{f_0} \tag{12}$$

is constant for any m.

The distribution of the occupied bands of the sampled waveform $h_S(t)$ is shown in Fig. 3. It can be recognized that reconstruction of $h(t)$ by bandpass filtering the fundamental spectrum is allowed if

$$\frac{B}{f_0} \leq 1 \tag{13}$$

since this condition ensures no overlapping between $m = 1$ and $m \neq 1$ spectra.

When $h(t)$ is not phase modulated, i.e., has the form (3′), samples result of uniform time spacing and width. The harmonic spectra all have the same bandwidth, and reconstruction of $h(t)$ by bandpass filtering now requires the condition

$$\frac{B}{f_0} \leq 2. \tag{14}$$

V. Design of the Tapping Transducers

The above analysis has demonstrated how the phase-sampling procedure permits the synthesis of a given impulse-response function. We shall now describe how a planar con-

[2] In the limit theoretical case of an instantaneous sampling [$\rho = 0$ in (7)], a weighting factor must be introduced in the amplitude of the δ-function samples to ensure constance of the sample energy as $\rho \to 0$. As remarked by Tancrell [13], the weighting factor of the sample at the time t_n is inversely proportional to the instantaneous frequency $\phi'(t_n)$ of $h(t)$ at t_n (the apex denotes the derivative with respect to time). This follows by substituting in (5) the identity $\delta[\phi(t) - n\pi] = \delta(t - t_n)/|\phi'(t_n)|$.

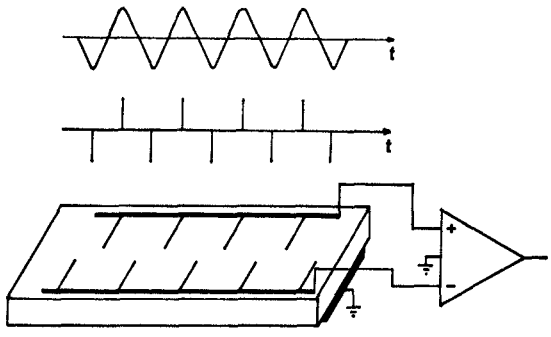

Fig. 4. Single-phase electrode grating synthesizing samples of constant amplitude and opposite polarity.

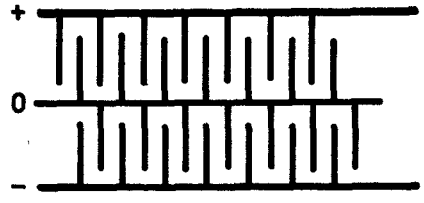

Fig. 5. Bipolar double array with a fish-bone-like coplanar reference electrode.

figuration of electrode transducers must be designed in order to implement the tapping structure of an ASW transversal filter with a phase-sampled impulse response.

A. Synthesis of Constant-Amplitude Impulse Responses

In piezoelectric materials, elastic surface waves are detected by the potential difference excited between a pair of electrodes interested by the electric field associated with the acoustic stress. Surface-wave tapping can be realized by depositing on the propagation surface an array of finger-like electrodes and picking up the voltage of each of these electrodes with respect to a ground electrode below the piezoelectric substrate [15], [16]. This type of transducer, referred to as a "single-phase" electrode transducer, acts as a linear antenna collecting the piezoelectric field traveling beneath. The sets of positive and negative samples of a constant-amplitude impulse response are synthesized by two coplanar single-phase gratings of constant-aperture electrodes, spaced according to the sample intervals, that are connected, respectively, to the noninverting and inverting input of a differential amplifier (Fig. 4).

Single-phase electrode transducers, however, have been found to be less efficient than "alternate-phase" transducers, where a reference electrode is inserted directly on the propagation surface, parallel to the tapping electrodes; in fact, in this case the distribution of the electric field between the electrodes interests essentially the same volume of the surface waves, and does not depend on the thickness of the substrate [16], [17].

A planar structure equivalent to the single-phase double array illustrated above is shown in Fig. 5. The two electrode gratings are now faced to a coplanar reference electrode resembling a fish bone. The intermediate electrodes between the fingers of each array must be colinear with the fingers of the array of opposite polarity in order to keep the periodicity of the electric-field distribution. This transducer geometry requires a balanced input/output network. When the samples have uniform amplitude, however, the structures of the two double arrays are identical, and only one of them can be used. The resulting configuration is the classical scheme of the "interdigital" transducer, which does not require a balanced network.

In order to understand how this simple structure provides the required sampled impulse response, consider a surface-elastic impulse propagating along the array. When the impulse passes beneath an electrode, the associated electric field induces a charge on it that determines a potential difference between the two combs. When the impulse interests an electrode of the other comb, a charge of the same sign is induced, and an opposite potential difference results. The impulse response of the interdigital array therefore consists of a sequence of positive and negative pulses, whose time configuration is the image of the spatial pattern of the array.

An alternative configuration equivalent to the fish-bone structure is shown in Fig. 6. The teeth of the two noninterleaved combs are now faced to a coplanar reference electrode having the form of a meander line folded around them, and passing in correspondence of the zero-crossing points of the impulse-response function. This geometry permits us to interleave the two combs, obtaining the configuration shown in Fig. 7(b). Although the resulting electric-field distribution (Fig. 7) is similar to that obtained with an interdigital array of the same periodicity (Fig. 8), a 3-dB-efficiency improvement is obtained by the insertion of the meander-like ground electrode. In Fig. 9 is shown the amplitude versus frequency response of a transmitting–receiving pair of such transducers, each operating at 4 MHz with a 3-dB bandwidth of 2 MHz. One can remark the noticeable exaltation of the third-harmonic response, a feature that can have interesting applications for overtone transducer operation.

B. Synthesis of Amplitude-Modulated Impulse Responses

The synthesis of amplitude-modulated impulse responses can be achieved by single-phase electrode transducers using an arrangement similar to that shown in Fig. 4 with the finger active lengths graded proportionally to the sample weights $a(t_n) = a_n$. In fact, the active length of each electrode, i.e., the length facing the reference electrode below the substrate, determines the amplitude of its impulse response.

When a coplanar fish-bone-like reference electrode is inserted in this structure (Fig. 10), each finger of the two combs is surrounded on either side by the reference electrode. The basic assumption is made that the response from one finger is proportional to the length of this finger facing the adjacent electrodes. In fact, when an elastic impulse passes beneath a finger, it can be reasonably assumed that the charge induced on it by the electric field associated with the impulse depends on its length facing the adjacent electrodes on both sides, and hence the excited potential difference has a value proportional to this facing length. This assumption is substantially confirmed by the experimental observations.

Consider a finger of one comb at the position x_n (Fig. 10). If z_n is its aperture, its total facing length is $2z_n$. If z_n is made proportional to a_n, i.e., $z_n = Ka_n$, with K a suitable constant, the finger response also results proportional to a_n. On the other hand, the colinear finger of the fish bone faces in turn on either side finger of the other comb. If $z_{n-1} = Ka_{n-1}$ and

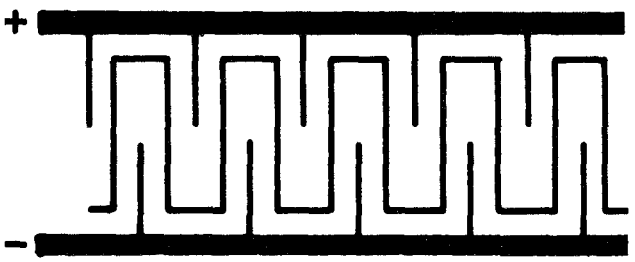

Fig. 6. Bipolar noninterleaved arrays with a meander-like coplanar reference electrode.

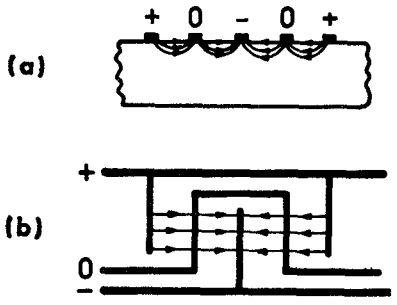

Fig. 7. Pictorial representation of the electric-field distribution in bipolar interleaved arrays with meander-like ground electrode. (a) Side view. (b) Top view.

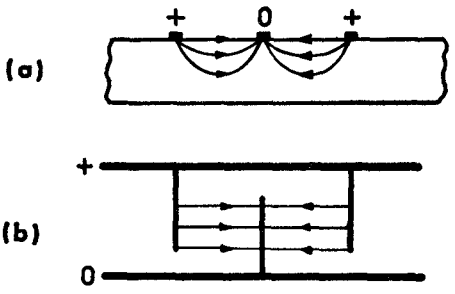

Fig. 8. Pictorial representation of the electric-field distribution in an interdigital transducer. (a) Side view. (b) Top view.

$z_{n+1}=Ka_{n+1}$ are the apertures of these side fingers, the total facing length is $z_{n-1}+z_{n+1}=K(a_{n-1}+a_{n+1})$. Hence, the overall response of the two colinear fingers at x_n is the sum of two in-phase contributions proportional to

$$2z_n + z_{n-1} + z_{n+1} = 2K\left(a_n + \frac{a_{n-1} + a_{n+1}}{2}\right). \quad (15)$$

The difference with respect to the desired weight a_n results negligible only if the value of a_n does not significantly differ from the average value $(a_{n-1}+a_{n+1})/2$ of the weights of the adjacent taps. When this difference is too large, the correct weights can be obtained by designing the lengths z_n of the fingers of the two combs so that the response at x_n results in

$$2z_n + z_{n-1} + z_{n+1} = \gamma a_n \quad (16)$$

with γ constant.

Hartemann and Dieulesaint [5], [6] implemented ASW filters of amplitude-modulated impulse responses using a structure resembling half of the double array in Fig. 10, with

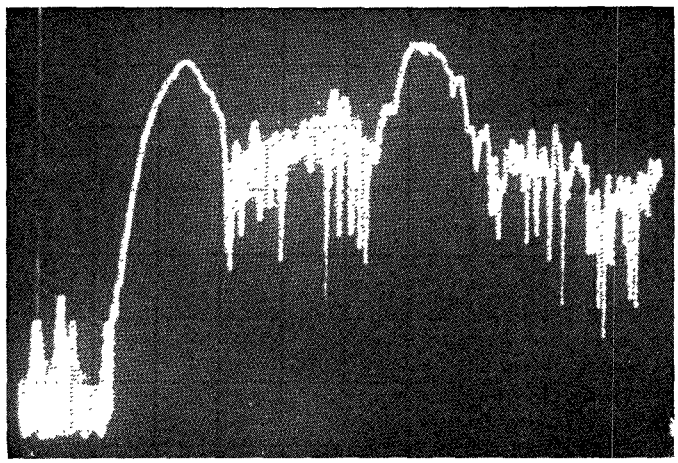

Fig. 9. Spectrum-analyzer display of the $(\sin^2 x)/x^2$-shaped amplitude response of a transmitting–receiving pair of bipolar interleaved arrays of constant pitch with meander-like ground electrode. Each array operates at 4 MHz with a 3-dB bandwidth of 2 MHz. Bulk wave responses can be observed between the first and third harmonic. Vertical scale: 10 dB/div. Horizontal scale: 2 MHz/div. Center frequency: 9.2 MHz.

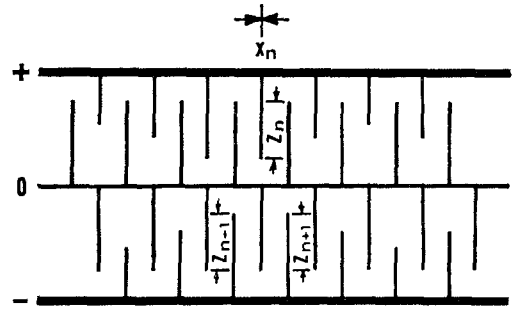

Fig. 10. Bipolar array of length-modulated fingers with fish-bone reference electrode.

the fingers of one comb graded in length proportionally to the amplitudes of the samples of one sign. In this case, the response of the length-modulated fingers provides samples of the same polarity having the desired amplitudes, while the response of the constant-length fingers provides samples of the opposite polarity having amplitudes equal to the average of those of adjacent fingers.

An alternative configuration is obtained by eliminating the reference electrode and interleaving the two combs (Fig. 11). In this structure, each finger directly faces two fingers of the other comb. With reference to Fig. 12, let Δz_{n-1}, Δz_n, and

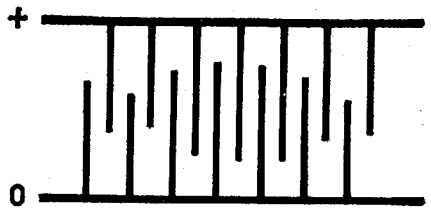

Fig. 11. Interdigital array with length-modulated fingers.

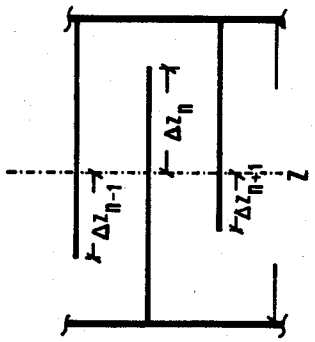

Fig. 12. Elementary cell of an interdigital array with length-modulated fingers.

Δz_{n+1} be the lengths of three adjacent fingers exceeding the middle line of the two combs. It can be easily recognized that the total facing length of the nth finger is

$$2\Delta z_n + \Delta z_{n-1} + \Delta z_{n+1}. \tag{17}$$

By arguments parallel to those used above, the response of the nth finger is assumed proportional to this quantity. Also in this case, therefore, the variation of the finger lengths must be designed so that the total facing length (17) results proportional to the required weight a_n. However, when

$$a_n \simeq \frac{a_{n-1} + a_{n+1}}{2} \tag{18}$$

as it always results for impulse responses having low fractional bandwidth, the required weight is achieved simply by making Δz_n proportional to a_n. Thus when condition (18) is met, the total length of the nth finger results in

$$z_n = \frac{Z}{2} + Ka_n \tag{19}$$

where Z is the distance of the two comb collectors (Fig. 12), i.e., is a linear function of the corresponding tap weight. A different method for implementing the tap weights by varying the finger lengths was described by Tancrell and Holland [8].

C. Synthesis of Discrete-Phase-Coded Impulse Responses

A class of impulse responses that can be simply synthesized by ASW transversal filters is that of waveforms having phase discontinuities. The feature of these waveforms is that adjacent samples around a phase discontinuity can have the same sign.

Consider, for instance, the waveform shown in Fig. 13(a), which exhibits a phase inversion at the time $\bar{t}$. The samples at times t_p and t_{p+2} [corresponding to the values $p\pi$ and $(p+2)\pi$ of the instantaneous phase] have the same sign [Fig. 13(a)], and hence the corresponding taps must have the same polarity. The simplest means of synthesizing this phase inversion

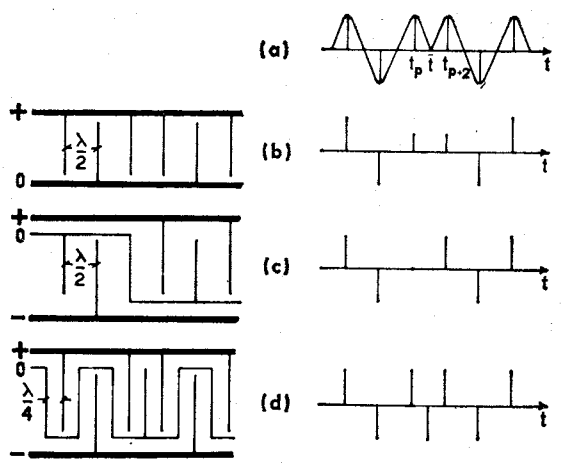

Fig. 13. (a) Phase inversion of a constant carrier waveform. Samples at the times t_p and t_{p+2} have the same sign. (b)–(d) Various transducer configurations for the implementation of phase inversion (left) and expected impulse responses (right).

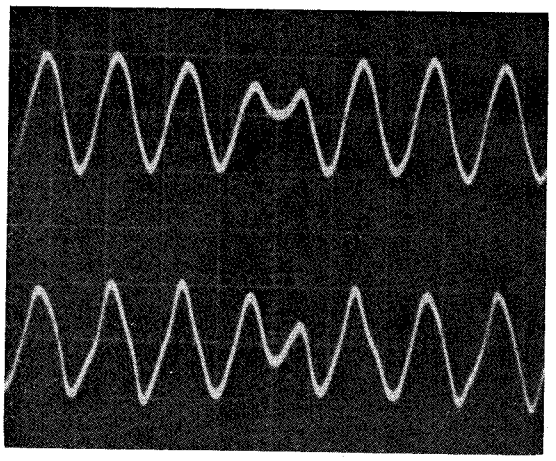

Fig. 14. Phase inversion experimentally obtained using the configuration of Fig. 13(b) (upper trace) and that of Fig. 13(d) (lower trace).

appears to be the construction of an interdigital array having two consecutive fingers connected to the same collector [Fig. 13(b)]. It has been observed, however, that this arrangement fails to provide the required impulse response, since two consecutive electrodes of the same potential bound an inactive gap in the array [7], [18]. According to our operation model, this impaired performance consists in the fact that the amplitude of the impulse response of each of these finger pairs is one half that of the other fingers [Fig. 13(b)]. In fact, each finger of the inversion pair faces only on one side a finger of the opposite comb, while all other fingers are facing on both sides. Evidence of this fact is given by the experimental response in Fig. 14.[3]

Squire *et al.* [7] synthesized phase inversions using the structure schematically shown in Fig. 13(c). In our opinion, the impulse response of the electrode that is run between the fingers of the array in correspondence of the inversion point is zero. The reason for this is the same as for the zero response of the meander reference electrodes in the transducer illustrated in Fig. 8, i.e., this electrode determines a balanced potential difference between the leads of the two adjacent

[3] Another proof of the influence of the facing length on the impulse-response amplitude is given by the fact that the first and the last finger of an array also provide about half the amplitude of the internal fingers when the rise time of the system is small with respect to half a period of the carrier.

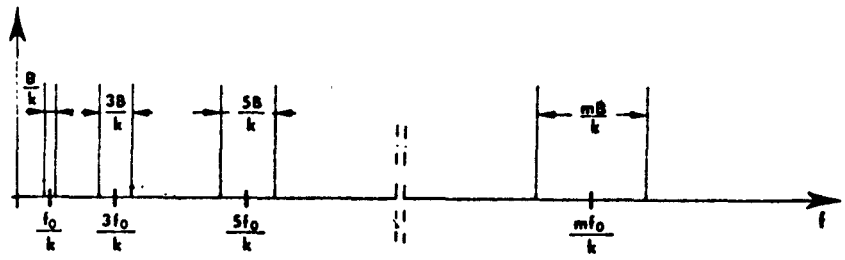

Fig. 15. Spectral band distribution obtained by sampling a kth subharmonic of $h(t)$. The kth spectrum coincides with that of $h(t)$.

fingers. According to our model, the set of samples that corresponds to this arrangement is that shown in Fig. 13(c).

The bipolar structure of interleaved fingers with a meander-like reference electrode described above seems suited to provide phase inversion using the configuration shown in Fig. 13(d). However, it can be recognized that the meander finger corresponding to the inversion point, facing electrodes of the same comb, provides an impulse response of the same amplitude and opposite sign of that of the inversion finger pair [Fig. 13(d)]. The phase inversion is obtained in this manner by a sudden frequency change. The experimental response shown in Fig. 14 confirms approximately the predicted behavior.

Thus far, for the sake of simplicity, we have limited our considerations to impulse responses with linear PM law. When the PM is not linear, the time interval and width of the samples are not uniform, and the spatial interval and width of the corresponding tapping electrodes must be accordingly graded. The edges of the nth electrode must be located at the positions

$$x_{n1} = X + vt_{n1}$$
$$x_{n2} = X + vt_{n2} \tag{20}$$

where x is the direction of surface-wave propagation, v is the propagation velocity, X is an arbitrary reference, and $t_{n1,2}$ are given by (7).

It must be noted that the top of the samples considered in Section IV is graded according to the shape of the corresponding section of the envelope $a(t)$ (Fig. 2). This shaping, however, cannot be realized by the tapping electrodes, since the metal strips are equipotential. Electrodes thus synthesize samples with a flat top, but the difference is negligible if the value of ρ in (7) is suitably less than π, i.e., if the electrode width is small with respect to the electrode spacing.[4]

The above design of the tapping electrodes is based on a simplified model of the physical process of surface-wave generation and detection. We have assumed that electrodes act essentially as ideal sensors, i.e., work as low-coupled nonreflecting taps capable of exciting or detecting a potential distribution corresponding to their geometrical configuration. Experiments confirm the existence of the predicted harmonic responses, but show obviously noticeable discrepancies in the values of the amplitude of these harmonic components with respect to the Fourier coefficients (9). These coefficients, in fact, have been derived merely using signal-analysis concepts, without regard for the physical operation of surface-wave tapping. A rigorous investigation of the actual physical operation would require the solution of the coupled electromechanical equations subject to the boundary conditions [16]. This problem has been investigated by several authors [16], [20]–[22] for interdigital structures of constant electrode pitch, width, and aperture and introducing simplifying assumptions. Various evaluations were obtained for the relative amplitudes of the harmonic components coupled to the transducer geometry. The evaluation of these amplitudes for an array of nonuniform pitch and with fingers graded in size appears extremely difficult, and is beyond the scope of the present work. In spite of this fact, ASW filters constructed following the above design criterion exhibit responses in sufficiently good agreement with the theoretical predictions, and this seems to suggest that the actual operation of surface-wave tapping transducers is not too far from the simplified model described here.

[4] The investigation of the influence of this approximation on the desired transfer function would require the evaluation of the spectrum of the sampled impulse response with flat-top samples. If samples are uniform in spacing and width, it is known that the spectrum of the reconstructed waveform results, weighted by the Fourier transform of the sampling pulse [19]. Hence, to reduce distortion, the pulsewidth must be suitably small for the corresponding bandwidth to be large in comparison with the maximum frequency of the required transfer function. One can reasonably assume that an analogous condition holds in the case of nonuniform sampling pulse width, and therefore the maximum sample width must be dimensioned according to the operation bandwidth.

VI. Reduction of the Tap Number

The investigation of the number of samples required for the synthesis of a specified impulse response leads to interesting results.

From (4), this number comes out to be equal to the number of π-increments of $\phi(t)$ in the time interval T, i.e.,

$$N = \frac{1}{\pi}\left[\phi\left(\frac{T}{2}\right) - \phi\left(-\frac{T}{2}\right)\right] \tag{21}$$

where $\phi(t)$ has been assumed a single-valued function of t. If $\bar{f}$ is the time average of the instantaneous frequency $f(t) = (1/2\pi)(d\phi(t)/dt)$, given by

$$\bar{f} = \frac{1}{T}\int_{-(T/2)}^{T/2} f(t)\,dt = \frac{1}{2\pi T}\left[\phi\left(\frac{T}{2}\right) - \phi\left(-\frac{T}{2}\right)\right] \tag{22}$$

the number (21) can be simply written as

$$N = 2\bar{f}T. \tag{23}$$

The spectral distribution of the sampled impulse response derived in Section IV suggests, however, that any one of the harmonic waveforms of the series (10) can be generated from the sample sequence by bandpass filtering the corresponding spectrum, provided that this is not overlapped by the others. Let us consider then a set of samples whose fundamental spectrum is a kth subharmonic (with k odd) of the given impulse response $h(t)$ (3).

The kth harmonic spectrum of this set of samples coincides with the spectrum $H(f)$ of $h(t)$ (Fig. 15), and therefore, provided that this spectrum is not overlapped by the others, the

reconstruction of $h(t)$ from this sample set is allowed. It follows that the sample number (23) is redundant and can be reduced. In fact, phase sampling of the subharmonic waveform

$$h_k(t) = a(t) \cos\left[\frac{1}{k}\phi(t)\right] \tag{24}$$

leads to a number of sampling points

$$N_k = 2\frac{\bar{f}}{k}T \tag{25}$$

occurring at the times where

$$\frac{1}{k}\phi(t) = n\pi, \qquad n = \text{integer} \tag{26}$$

and thus coinciding with one every k of the sampling points given by (4).

From Fig. 15 it can be easily derived that the kth spectrum is not overlapped by any other if

$$\frac{B}{f_0} \leq \frac{2}{k+1}. \tag{27}$$

Hence, for a given fractional bandwidth B/f_0, the maximum value k_M of k results in the maximum odd integer contained in

$$2\frac{f_0}{B} - 1. \tag{28}$$

For the sake of simplicity, let us assume that f_0/B is an integer [so that the number (28) is odd] and that f_0 coincides with $\bar{f}$. Then, from (25) and (28), the minimum sample number results in

$$N_{\min} = BT\frac{1}{1 - \dfrac{B}{2f_0}}. \tag{29}$$

From the above arguments it follows that the minimum number of samples that permits the reconstruction of $h(t)$ depends on its fractional bandwidth B/f_0. According to the condition (13), the phase-sampling procedure cannot be applied if B/f_0 exceeds unity. When B/f_0 is contained in the range

$$1 \geq \frac{B}{f_0} > \frac{1}{2}$$

the sample number is given by (23). A reduction of this number is allowed only if $B/f_0 \leq 1/2$. Note that whatever is the fractional bandwidth in the interval

$$\frac{1}{q} \geq \frac{B}{f_0} > \frac{1}{q+1}$$

the maximum odd integer in (28) is $2q-1$, so that the minimum sample number is always

$$N_{\min} = \frac{2\bar{f}T}{2q-1}.$$

From (29) it appears that, for a given bandwidth B, $N_{\min}$ has a value contained in the range

$$2BT > N_{\min} > BT$$

depending on the value of $f_0 \geq 2B$. When $f_0 \gg 2B$, $N_{\min}$ is very close to BT.

In the case of the constant carrier-frequency waveform (3'), we have shown by similar arguments [9] that the minimum sample number is obtained by dividing the number (23) (where $\bar{f}$ coincides now with the value of the carrier frequency f_0) by the maximum odd integer contained in the ratio

$$\frac{2f_0}{B}. \tag{30}$$

In the particular case that this ratio is itself an odd integer, the minimum sample number becomes exactly BT.

The possibility of reducing the number of the impulse-response samples, and hence the number of the tapping electrodes in an ASW transversal filter, can have attractive applications for several reasons. First of all, when the operation frequency of ASW filters is extended up to microwaves, the resolution and the definition of an electrode pattern designed at a fundamental frequency become extremely hard to achieve using both electron-beam as well as photolithographic fabrication. Moreover, the effect of coupling and mutual interaction between the electrodes rapidly grows with the electrode number. A reduction of this number would yield a simplified design and an easier implementation of the device [23]. On the other hand, a reduction of the tap number has its counterbalance in a reduction of the output signal due to the decrease of the harmonic-spectra amplitudes. In principle, the signal-to-noise ratio of an ASW filter is not affected by the amplitude of the filter transfer function. However, the reduction of the output signal limits the dynamic range of the device, which is a basic requirement in weak signal-processing systems. Hence, the advantages of adopting a reduction factor $k \leq k_M$ must be evaluated by taking into account the dynamic-range degradation that can be tolerated.

The form of the Fourier coefficients (9) predicts that the amplitudes of the harmonic responses depend on the transducer geometry in terms of the electrode width-to-period ratio. As mentioned above, however, the values of these coefficients are not reliable, since they do not take into account the physical nature of ASW devices. The actual dependence of the harmonic responses on the electrode width-to-period ratio has been both theoretically and experimentally investigated only for arrays of electrodes of constant period, width, and aperture [16], [20]–[22], [24]. Further investigation is needed, however, for more complicated geometries. It is to be remarked that the interdigital transducer with a meander-like reference electrode, described in the previous section, can represent an interesting means for third-harmonic transducer operation. The response shown in Fig. 9 was obtained making the electrode width equal to one eighth of the acoustic wavelength.

VII. Application of ASW Filters to Signal Passive Generation and Matched Filtering

Because of their capability of synthesizing complicated impulse responses, ASW filters represent a powerful tool for signal passive generation and matched filtering [4]. A very attractive feature of such devices is, moreover, that one and the same filter can be used to perform both these functions.

A. Signal Passive Generation

The approach of generating a signal from a filter having this signal as the impulse response is referred to as "passive" generation. When impulsing a transversal filter designed according to the phase-sampling procedure, its time response is described by the series (10). In principle, each of the terms of this series can be generated by selecting the corresponding spectrum at the output of the device, provided that this spectrum is not overlapped by the others. Thus passive generation permits us to obtain from the same filter one or more signals having the same structure, but extending over different frequency bands.

The tap configuration that synthesizes the sampled impulse response (10) can be written as

$$h_S\left(\frac{x}{v}\right) = a\left(\frac{x}{v}\right) \sum_{1\ m\ \text{odd}}^{\infty} C_m \cos\left[m\phi\left(\frac{x}{v}\right)\right], \qquad -\frac{L}{2} \le x \le \frac{L}{2} \tag{31}$$

where x is the coordinate along the delay line, v is the propagation velocity, and $L=vT$ is the length of the delay line. When driving the line by an impulse $\delta(t)$ from the input 1 ($x=-(L/2)$) (Fig. 1), the response is, apart from a constant time delay

$$\begin{aligned} r_1(t) &= \left[\int_{-\infty}^{\infty} \delta(t-\xi)h_S(\xi)\,d\xi\right] \otimes g(t) \\ &= h_S(t) \otimes g(t) \end{aligned} \tag{32}$$

where $\xi=x/v$, the symbol $\otimes$ denotes the convolution operation, and $g(t)$ represents the impulse response of the cascaded bandpass filter. The convolution (32) can be written as the Fourier transform of the product of the overall spectrum $H_S(f)$ of $h_S(t)$ by that of $G(f)$ of the bandpass filter, i.e.,

$$r_1(t) = \int_{-\infty}^{\infty} H_S(f)G(f)e^{j2\pi ft}\,df. \tag{33}$$

If $G(f)$ selects the band $m(f_0-(B/2)) \div m(f_0+(B/2))$ occupied by the mth harmonic spectrum $H^m(f)$, the output waveform is the mth harmonic term $h^m(t)=C_m a(t)\cos[m\phi(t)]$ of the series (10), i.e.,

$$r_1(t) = \int_{-\infty}^{\infty} H^m(f)e^{j2\pi ft}\,df = C_m a(t)\cos[m\phi(t)]. \tag{34}$$

B. Signal Matched Filtering

Signal passive generation is particularly advantageous in correlation receivers, as in radar, sonar, and digital communication systems, where the basic problem is the correlation of a given signal $s(t)$ by means of a filter having conjugate characteristics. Such a filter, referred to as a "matched" filter, must have a transfer function that is the complex conjugate of the spectrum $S(f)$ of $s(t)$:

$$H(f) = \gamma S^*(f) \tag{35}$$

with γ a real constant, i.e., an impulse response that is the time reverse of the signal $s(t)$:

$$h(t) = \gamma s(-t). \tag{36}$$

A noticeable feature of transversal filters is that their impulse response $h_S(t)$ becomes $h_S(-t)$ when reversing the direction of the input signal propagation in the delay line. In fact, the delay line shown in Fig. 1 has two input ports,[5] and taps are scanned in one sense or the other depending on which port is used as the input. This feature yields that the same filter used for passive generation of a signal by impulsing the delay line from input 1 can be used for matched filtering the same signal simply by applying it to input 2. This capability offers the important advantage that the matched filter tracks the signal even if the delay times drift for temperature variations or other causes.

When the filter is driven with the signal $h^m(t)$ (34) from port 2 ($x=L/2$), the response is, apart from a constant time delay

$$\begin{aligned} r_2(t) &= \int_{-\infty}^{\infty} h^m(t+\xi)h_S(\xi)\,d\xi \\ &= \int_{-\infty}^{\infty} h^m(t-\xi)h_S(-\xi)\,d\xi \\ &= \int_{-\infty}^{\infty} H^m(f)H_S{}^*(f)e^{j2\pi ft}\,df. \end{aligned} \tag{37}$$

Since the product $H^m(f)H_S{}^*(f)$ is zero outside the band $m(f_0-(B/2)) \div m(f_0+(B/2))$, where $H_S(f)=H^m(f)$, the response (37) becomes

$$\begin{aligned} r_2(t) &= \int_{-\infty}^{\infty} |H^m(f)|^2 e^{j2\pi ft}\,df \\ &= C_m{}^2 \int_{-\infty}^{\infty} h^m(t-\xi)h^m(\xi)\,d\xi \end{aligned} \tag{38}$$

which is the autocorrelation function of $h^m(t)$.

VIII. Experimental Models

In this section we describe experimental models of ASW filters, all constructed on quartz and operating at relatively low frequency. In all experiments the input signal was launched using a broad-band transducer.

A. Dispersive Filters

The synthesis of dispersive characteristics is one of the more interesting applications of ASW filters, because of the extreme simplicity of this method with respect to conventional techniques. The previous theory is applied here to the design of two types of dispersive filters: one having a linear group delay versus frequency characteristic and the other a hyperbolic one. The first step for the filter design is to derive in the time domain the impulse response corresponding to the characteristics assigned in the frequency domain. This is performed by calculating the inverse Fourier transform of the required transfer function, which, if not possible otherwise, can be evaluated by numerical computation.

Linear Group Delay versus Frequency Characteristic: Using the principle of stationary phase [14], it can be shown that a linear group delay versus frequency characteristic with a con-

[5] Note that a transversal filter is a three-port reciprocal structure, i.e., its transfer function does not change by exchanging the output with the input.

stant amplitude response corresponds approximately to the rectangular-envelope linear FM impulse response

$$h(t) = \cos\left[2\pi\left(f_0 t + \frac{\alpha}{2}t^2\right)\right], \qquad \text{for } |t| \le \frac{T}{2}$$
$$= 0, \qquad \text{elsewhere} \qquad (39)$$

where α is the FM rate. From (4), the sampling points are given by the times t_n, where

$$2\pi\left(f_0 t + \frac{\alpha}{2}t^2\right) = n\pi, \qquad n = \text{integer}$$

that provides

$$t_n = -\frac{f_0}{\alpha} + \sqrt{\left(\frac{f_0}{\alpha}\right)^2 + \frac{n}{\alpha}}, \qquad |t_n| \le \frac{T}{2}.$$

Since the envelope of the impulse response (39) is constant, i.e., $a(t_n) = 1$, for any n, the electrodes of the array must all have the same aperture. From (7), the electrode edges must be located at the positions corresponding to the times

$$t_{n1,2} = -\frac{f_0}{\alpha} + \sqrt{\left(\frac{f_0}{\alpha}\right)^2 + \frac{1}{\alpha}\left(n \mp \frac{\rho}{2\pi}\right)}, \qquad \rho < \pi.$$

The signal characteristics used in an experimental device (25) were the following:

center frequency	$f_0 = 9$ MHz
bandwidth	$B = 2.5$ MHz
time duration	$T = 32\ \mu$s.

Since for linear FM the average frequency $\bar{f}$ (22) coincides with the center frequency f_0, the finger number (23) for fundamental frequency operation is $N = 576$. The fractional bandwidth being less than 50 percent, this number can be reduced. From (28), the maximum reduction factor is $k_M = 5$, and the minimum finger number results in $N_{\min} = 115$.

An interdigital array for fundamental frequency operation was constructed for the value $\rho = \pi/2$. Broad-band transmitter arrays were deposited at both ends of the receiving transducer to realize the two input-port structures described in Section VII. The measured group delay and amplitude versus frequency characteristics are shown in Fig. 16.

The signal (39) has important applications in pulse-compression techniques [4], where the fundamental problem is the synthesis of the phase equalizer for signal matched filtering. As discussed in Section VII, the two-input structure of ASW filters provides the means for both signal generation and matched filtering. In Fig. 17 are shown the passive-generated linear FM signal and its correlation pulse.

Harmonic operation was tested by constructing interdigital arrays for the reduction factors $k = 3$ and $k = 5$, having the same finger width as before.[6] In Fig. 18 the details of the correlation pulses obtained by feeding with the same linear FM

[6] The finger width in the reduced array cannot be increased to $k\rho$ as it could be if the array was designed for its own fundamental frequency operation, since, as discussed,[4] the maximum finger width must be dimensioned to the actual operation bandwidth.

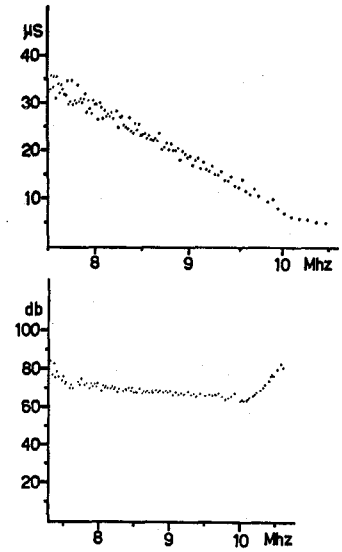

Fig. 16. Frequency response for a linear-dispersive transducer. Top: measured group delay versus frequency characteristic. Bottom: measured amplitude versus frequency characteristic.

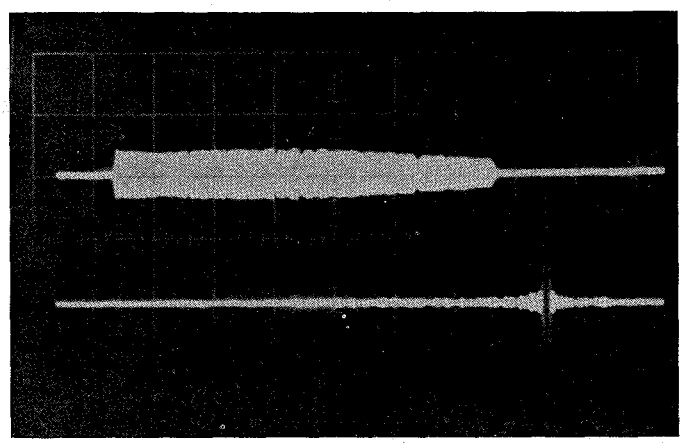

Fig. 17. Linear-dispersive transducer. Passive-generated signal (top) and correlation signal (bottom) (5 μs/div).

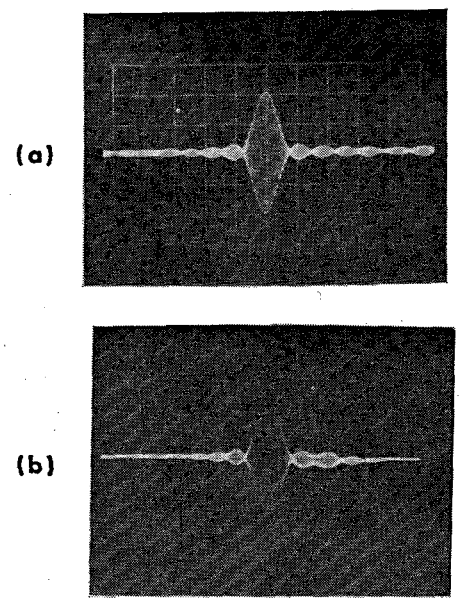

Fig. 18. Linear-dispersive transducer. Details of the correlation pulse from the filter with (a) $k = 1$ and (b) $k = 5$ (0.5 μs/div).

signal the filters with $k=1$ and $k=5$ are compared. The amplitude reduction resulted in ~19 dB.

Hyperbolic Group Delay versus Frequency Characteristic: Another signal of interest in correlation receivers is the linear period-modulated waveform

$$h(t) = \cos\left[\frac{2\pi}{b}\ln\left(1+\frac{b}{T_0}t\right)\right], \qquad \text{for } |t| \le \frac{T}{2}$$
$$= 0, \qquad \text{elsewhere} \qquad (40)$$

where b is the rate of the hyperbolic FM

$$f(t) = \frac{1}{T_0 + bt}. \qquad (41)$$

It can be shown, also using in this case the principle of stationary phase, that the group delay versus frequency characteristic of the related transfer function has a hyperbolic behavior [26]. The sampling times t_n are now given by

$$t_n = \frac{T_0}{b}\left[e^{(n(b/2))}-1\right], \qquad |t_n| \le \frac{T}{2}.$$

The finger edges correspond to the times

$$t_{n1,2} = \frac{T_0}{b}\left[e^{[n\mp(\rho/2\pi)]b/2}-1\right].$$

Also, in this case, the fingers of the interdigital array all have the same aperture because of the constant signal envelope. The characteristics of the experimental model are the following:

center frequency	$f_0 = 9$ MHz
bandwidth	$B = 2.5$ MHz
time duration	$T = 30\ \mu$s.

In this case, the center frequency f_0 does not coincide with the average instantaneous frequency $\bar{f}$, which can be calculated from (22) and (41). By inserting the value of $\bar{f}$ in (23), the tap number for fundamental frequency operation results in $N=533$. The value of the fractional bandwidth permits, however, a maximum reduction factor $k_M=5$, so that the minimum tap number is $N_{\min}=106$. The experimental group delay versus frequency response is shown in Fig. 19. In Fig. 20 are compared the correlation pulses from the filters operating at the fundamental and the fifth-harmonic frequency; the amplitude ratio is ~12 dB [27].

B. Bandpass Filters

The transfer function of an ideal bandpass filter, given by

$$H(f) = e^{-j2\pi f t_0}, \qquad \text{for } |f-f_0| \le \frac{B}{2}$$
$$= 0, \qquad \text{elsewhere} \qquad (42)$$

corresponds to the impulse response

$$h(t) = B\frac{\sin[\pi B(t-t_0)]}{\pi B(t-t_0)}\cos[2\pi f_0(t-t_0)] \qquad (43)$$

where t_0 is a constant group delay.

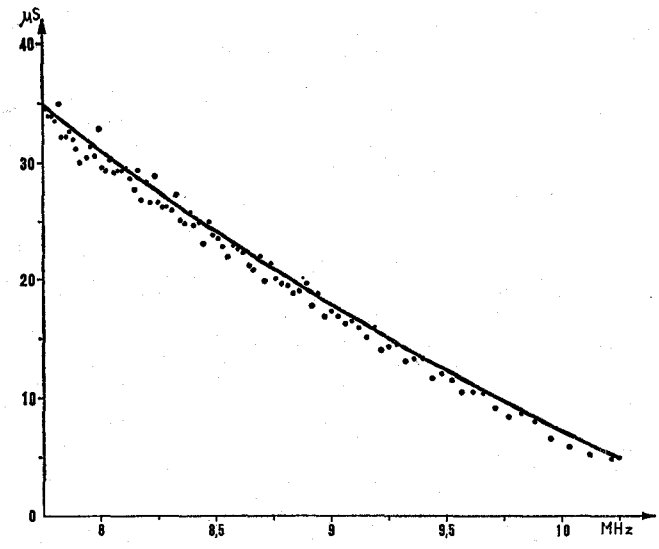

Fig. 19. Hyperbolic-dispersive transducer. Measured group delay versus frequency characteristic. Full line shows the expected delay.

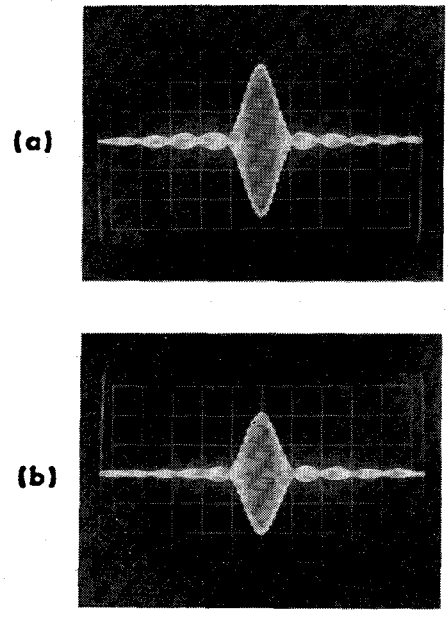

Fig. 20. Hyperbolic-dispersive transducer. Details of the correlation pulse from the filter with (a) $k=1$ and (b) $k=5$ (0.5 μs/div).

The preliminary consideration that must be made is that this impulse response extends indefinitely in time, while the synthesis of a physical filter necessarily requires its limitation to a finite duration. The need for truncating the impulse response corresponding to a transfer function assigned in a finite bandwidth is a general problem encountered when, as in ASW devices, the filter synthesis is performed in terms of its time-domain specification. Impulse-response truncation produces distortion in the frequency response that must be taken into account in the filter design. As is well known, the limitation of the impulse response (43) to a duration T around the time t_0 produces ripples in the passband an in the stopband, and affects the rapidity of the fronts at the bandedges. As T is increased, ripples in the middle of the passband and in the stopband lower, and the fronts become steeper. Since, however, the ideal transfer function (42) has discontinuities at the

cutoff frequencies $f=f_0 \pm B/2$, the magnitude of the ripples around the bandedges cannot be reduced even for increasing T because of the Gibbs' phenomenon [28].

Another feature that must be taken into account in ASW bandpass filter design is the inherent limitation of the stopband due to the multiplicity of the frequency response. As shown in Section IV, the overall frequency response consists, in this case, of a succession of passbands, each of width B, centered on the frequencies odd multiple of f_0. Hence, the upper stopband is limited to the frequency band $f_0+B/2 \div 3f_0-(B/2)$ that is not interested by the third harmonic. The width of the stopband depends, therefore, on the filter fractional bandwidth.

The array for the synthesis of the bandpass impulse response (43) must have constant period. The finger positions correspond to the sampling times

$$t_n = t_0 + \frac{n}{2f_0} \cdot$$

In this case, the fingers all have the same width, corresponding to the fraction ρ/π of the sampling interval $1/2f_0$, i.e., its edges correspond to the times

$$t_{n1,2} = t_n \mp \frac{\rho}{4\pi f_0} \cdot$$

In an interdigital configuration, the finger lengths must be designed so as to introduce the weights

$$a(t_n) = \left| \frac{\sin\left[n\pi \dfrac{B}{2f_0}\right]}{n\pi \dfrac{B}{2f_0}} \right| .$$

A bandpass filter model was designed for the following data [29]:

center frequency	$f_0 = 8.125$ MHz
bandwidth	$B = 1$ MHz.

Since the value of the fractional bandwidth is suitably low, the condition (18) is met, and therefore, as discussed in Section V, the length of the nth finger can be made linearly dependent on the weight $a(t_n)$. The array pattern designed for a duration $T=8/B$ is shown in Fig. 21. The number of fingers for this time duration is $N=130$. One can clearly distinguish that two consecutive fingers are connected to the same collector where a phase inversion of the carrier occurs, due to the sign change of the sin x/x function in (43). In Fig. 21 is shown the filter impulse response. It can be remarked that the peak-to-sidelobe ratio is lower than the expected one. This discrepancy is attributable to the nonuniform finger lengths, which, because of the nonuniform metallization of the substrate, progressively distort the impinging wave, changing its straight front into a concave one [30], [12]. An approach for the reduction of this distortion has been recently described [12], consisting of the insertion of extra fingers that serve to equalize the velocity across the aperture of the array. These extra fingers are colinear with the fingers of the array, but are connected to the opposite collector, and are inactive, since the adjacent fingers are at the same electrical potential.

The degradation of the peak-to-sidelobe ratio causes the increase of the ripple magnitude that can be observed in Fig.

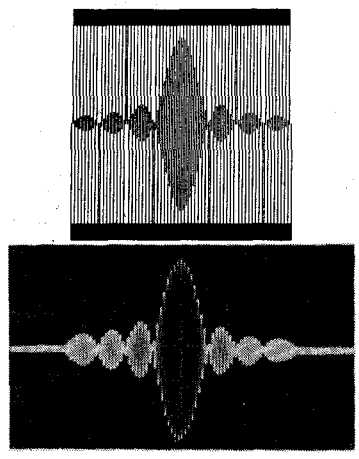

Fig. 21. Bandpass transducer. Top: tapping electrode configuration. Bottom: impulse response.

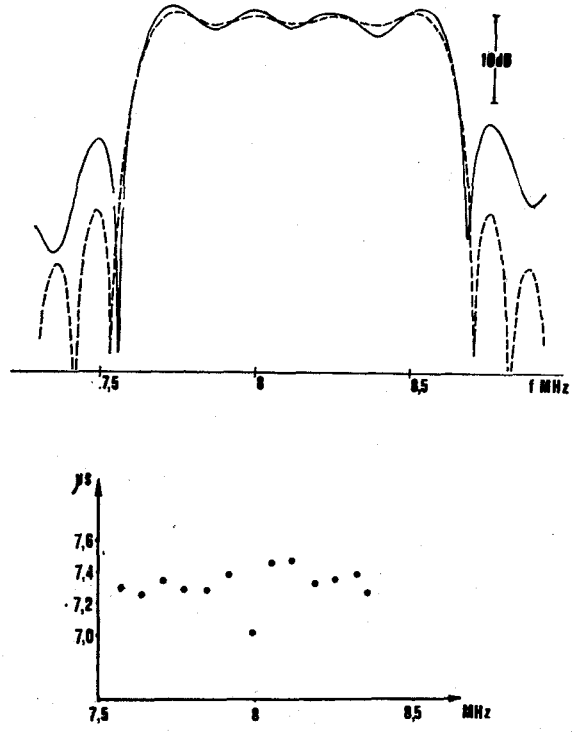

Fig. 22. Frequency response of the bandpass transducer. Top: amplitude versus frequency characteristic; theoretical (dotted line) and experimental (continuous line) behavior. Bottom: measured group delay versus frequency characteristic.

22 with respect to the theoretical behavior of the amplitude versus frequency response. In the same figure is shown the measured group delay versus frequency characteristic.

The panoramic view of the spectral response (Fig. 23) shows the presence of the third harmonic,[7] but also the existence of a spurious response around 15.5 MHz due to bulk-wave excitation. Unfortunately, this spurious response yields a further limitation of the filter stopband.

An ASW bandpass filter with a finger number reduced by the factor 3 was obtained by suppressing two fingers every three in the above mask. In Fig. 24 is shown its panoramic frequency response obtained with a launching transducer

[7] The asymmetric shape of the third-harmonic response is due to the weighting effect of the launching transducer, which has a bandwidth of about 4 MHz around 8 MHz.

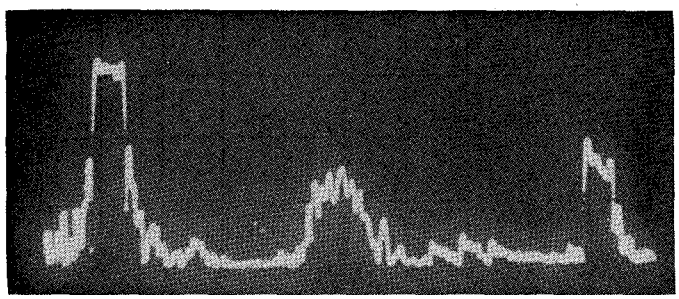

Fig. 23. Panoramic display of the amplitude versus frequency characteristic of the bandpass filter. Vertical scale: 10 dB/div. Horizontal scale: 2 MHz/div. Center frequency: 15.6 MHz.

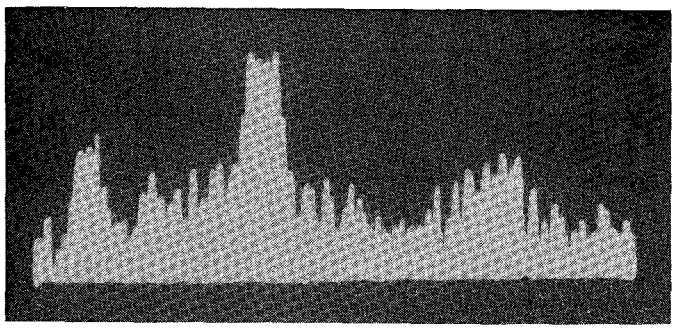

Fig. 24. Panoramic display of the amplitude versus frequency characteristic of the bandpass filter with $k=3$. Vertical scale: 10 dB/div. Horizontal scale: 2 MHz/div. Center frequency: 10.8 MHz.

working at 8 MHz. Ripples appear to be increased with respect to those obtained with the nonreduced array. This is mainly due to the failing validity of the approximation (18), in agreement with the fact that the fractional bandwidth of the fundamental spectrum is now three times as before. Better performance of the reduced array could be achieved by the rigorous design of the finger facing length described in Section V. It must be noted that in bandpass filter design, the reduction factor that can be adopted depends on the requirements on the stopband width, since the separation of the harmonic responses decreases as k is increased.

Several time-weighting functions have been devised [31], [32] capable of smoothing the ripples due to the Gibbs' phenomenon at the expense of a lower steepness of the fronts at the bandedges. By modifying the above finger weights according to the Fejér triangular function

$$w(t) = 1 - 2\frac{|t - t_0|}{T} \tag{44}$$

we obtained the frequency response shown in Fig. 25 [33]. Ripples appear reduced to less than 1 dB. By the use of more efficient weighting functions, as Lanczos' one [32], and by improving the electrode mask design, ripples as low as 0.1 dB could be achieved.

The inherent limitation of ASW bandpass filter applications is the stopband-width constraint imposed by the presence of the spurious responses due to bulk waves and of the harmonic responses. The amplitude of the harmonic responses can be minimized by a suitable choice of the electrode width-to-period ratio. A procedure for improving the stopband rejection can consist in the use of two cascaded bandpass arrays. This system cannot be implemented by directly using a pair of bandpass arrays as launching and detecting transducers. In fact, fingers of different lengths launch elastic

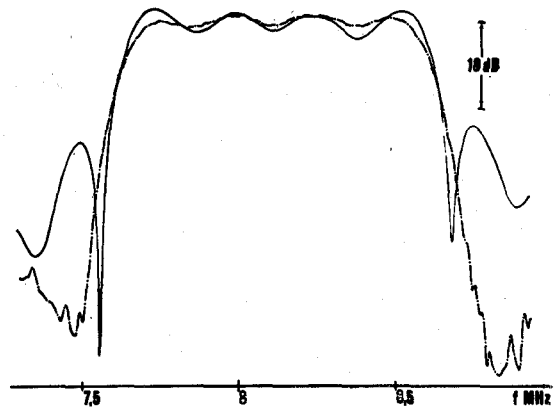

Fig. 25. Amplitude versus frequency response of the triangular-weighted bandpass filter (dotted line) compared with that of the unweighted filter (continuous line).

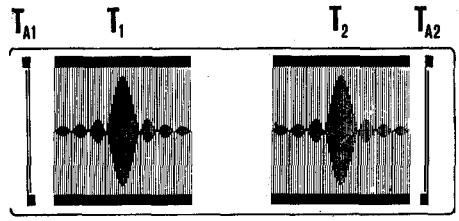

Fig. 26. Arrangement of cascaded bandpass array.

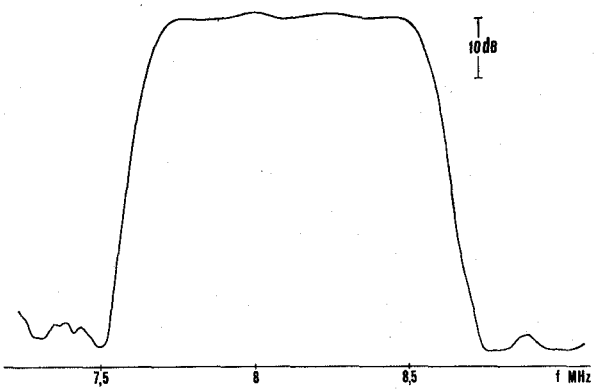

Fig. 27. Amplitude versus frequency response obtained by cascading two triangular-weighted bandpass filters.

waves having fronts of different aperture, which produce a nonuniform illumination of the receiving bandpass array. A means for overcoming this inconvenience is shown in Fig. 26. The electric signal collected by the broad-band transducer T_{A1}, illuminated by the wavefronts generated by the bandpass array T_1, is applied to the broad-band transducer T_{A2}, and finally detected by the second bandpass array T_2. An acoustic absorber, interposed between T_1 and T_2, avoids direct coupling of these arrays. The overall transfer function results in the product of the transfer functions of the single bandpass arrays. By this arrangement we have been able, using two triangular-weighted bandpass filters, to achieve the frequency response shown in Fig. 27. The bulk-wave response around 15.5 MHz was reduced to ~ -35 dB, while the rejection in the remaining stopband was as high as 60 dB. Ripples were not exalted, since the two arrays were designed slightly staggered in frequency, so that the overshoots in the amplitude versus frequency response of one coincided with the undershoots in the response of the other.

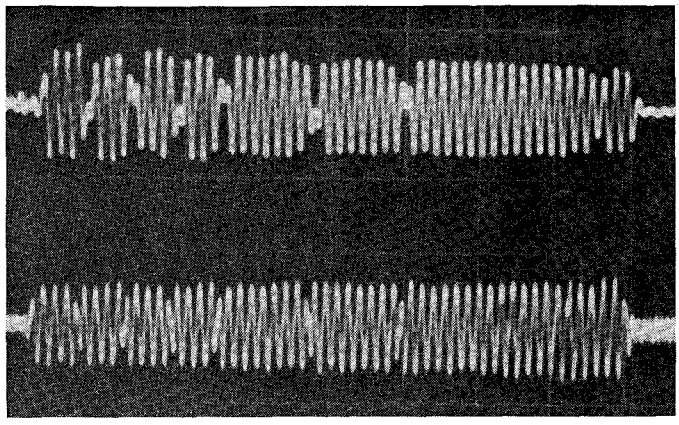

Fig. 28. ASW filter for processing a 13-b Barker-coded waveform. Impulse responses for the transducer geometries described in Fig. 13(b) (upper trace) and (d) (lower trace).

C. Discrete Phase-Coded Waveform Generator

As an example of the ASW filter application to the generation and correlation of discrete phase-coded waveforms, we experimented the synthesis of the classical 13-b Barker sequence [4] using the transducer geometries described in Fig. 13(b) and (d). Results on the generation of similar codes using the geometry of Fig. 13(c) have been reported elsewhere [34]. The arrays were designed for a carrier frequency of 4 MHz and a duration of 13 μs. Each bit contains, therefore, four RF cycles, generated by eight fingers. The phase inversions of the generated sequences (Fig. 28) exhibit the characteristics described in Section V. Third-harmonic distortion can be remarked in the waveform generated by the array with the meander reference electrode. As mentioned above, the exaltation of the third harmonic appears to be a feature of this type of transducer, as confirmed by the spectral response shown in Fig. 29. By selecting the appropriate band, sequences at 4 and at 12 MHz can both be generated from the same filter.

IX. Conclusions

It has been shown how ASW processors are inherently transversal filters, whose transfer function is determined by the configuration of a transducer array tapping the propagated acoustic signal. This is the reason why the application of the design procedure of linear transversal filters appears the most appropriate instrument for deriving the design of the tapping structure in ASW processors. This procedure requires the computation of the impulse-response function corresponding to the desired transfer function, and then the construction of a sampled version of this function. The time intervals, amplitudes, and sign of the samples determine, respectively, the spacing, weights, and polarity of the elements of the tapping structure. The particular nature of surface-wave tapping led to the development of an appropriate sampling procedure, according to which samples are taken where the required impulse response has the same instantaneous phase. The application of this procedure yields to a design of the tapping configuration that is in accordance with that derived using different approaches. Because of its generality, however, the described synthesis method provides a comprehensive derivation of the various aspects of ASW processor design and permits us, moreover, to deduct further features of this design.

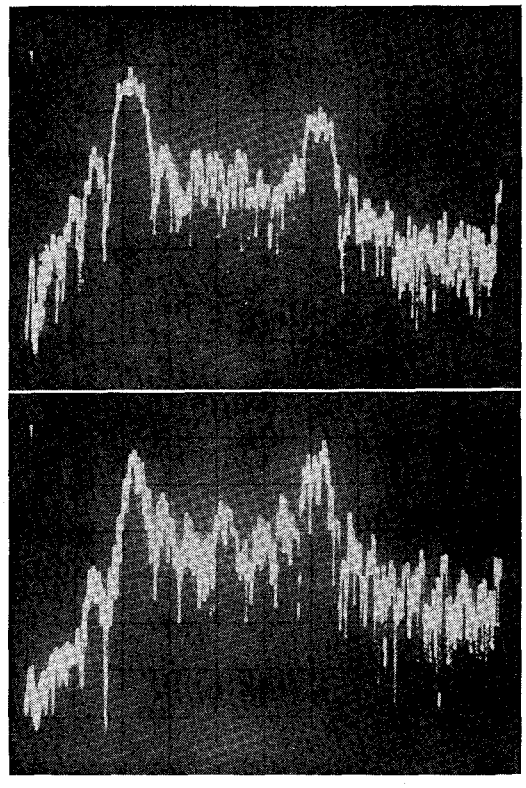

Fig. 29. ASW filter for processing a 13-b Barker-coded waveform. Panoramic display of the amplitude versus frequency characteristics for the transducer geometries described in Fig. 13(b) (upper trace) and (d) (lower trace). Vertical scale: 10 dB/div. Horizontal scale: 2 MHz/div. Center frequency: 9.6 MHz.

The extremely hard problem of investigating the physical mechanism by which elastic surface waves interact with the tapping structure is beyond the scope of this work. However, an elementary operation model was developed based on simplified assumptions and experimental evidence. Using this model, transducer geometries able to synthesize impulse responses of typical characteristics have been illustrated. Experiments conducted with these transducer geometries show a noticeable agreement with the expected results.

Finally, a purpose of this paper was to demonstrate the capability of implementing any complicated transfer function by ASW filters. When considering the present state of the art of surface-wave technology, one can envision that in the next years the potentiality of this new tool will find more and more applications, and ASW devices will be a common component of future electronic systems.

References

[1] J. H. Eveleth, "A survey of ultrasonic delay lines operating below 100 Mc/s," *Proc. IEEE*, vol. 53, pp. 1406–1428, Oct. 1965.
[2] R. M. White and F. W. Voltmer, "Direct piezoelectric coupling to surface elastic waves," *Appl. Phys. Lett.*, vol. 7, pp. 314–316, Dec. 1965.
[3] J. H. Rowen, "Tapped ultrasonic delay line and uses therefore," U.S. Patent 3 289 114, Nov. 29, 1966.
[4] C. E. Cook and M. Bernfeld, *Radar Signals*. New York: Academic Press, 1967.
[5] P. Hartemann and E. Dieulesaint, "Intrinsic compensation of sidelobes in a dispersive acoustic delay line," *Electron. Lett.*, vol. 5, pp. 219–220, May 1969.
[6] ——, "Acoustic surface wave filters," *Electron. Lett.*, vol. 5, pp. 657–658, Dec. 1969.
[7] W. D. Squire, H. J. Whitehouse, and J. M. Alsup, "Linear signal processing and ultrasonic transversal filters," *IEEE Trans. Microwave Theory Tech. (Special Issue on Microwave Acoustics)*, vol. MTT-

17, pp. 1020–1040, Nov. 1969.
[8] R. H. Tancrell and M. G. Holland, "Acoustic surface wave filters," *Proc. IEEE*, vol. 59, pp. 393–409, Mar. 1971.
[9] C. Atzeni and L. Masotti, "A new sampling procedure for the synthesis of linear transversal filters," *IEEE Trans. Aerosp. Electron. Syst.*, vol. AES-7, pp. 662–670, July 1971.
[10] H. E. Kallmann, "Transversal filters," *Proc. IRE*, vol. 28, pp. 302–310, July 1940.
[11] R. H. Tancrell *et al.*, "Dispersive delay lines using ultrasonic surface waves," *Proc. IEEE* (Lett.), vol. 57, pp. 1211–1213, June 1969.
[12] R. H. Tancrell and R. C. Williamson, "Wavefront distortion of acoustic surface waves from apodized interdigital transducers," *Appl. Phys. Lett.*, vol. 19, pp. 456–459, Dec. 1971.
[13] R. H. Tancrell, private communication.
[14] E. L. Key, E. N. Fowle, and R. D. Haggarty, "A method of designing signals of large time-bandwidth product," *IRE Int. Conv. Rec.*, pt. 4, pp. 146–155, 1961.
[15] R. M. Artz, E. Saltzmann, and K. Dransfeds, "Elastic surface waves in quartz at 316 MHz," *Appl. Phys. Lett.*, vol. 10, pp. 165–167, Mar. 1967.
[16] G. A. Coquin and H. F. Tiersten, "Analysis of the excitation and detection of piezoelectric surface waves in quartz by means of surface electrodes," *J. Acoust. Soc. Amer.*, vol. 41, pp. 921–939, Apr. 1967.
[17] J. de Klerk and R. M. Daniel, "Investigation to improve microwave acoustic delay lines," Final Rep., Contract F19628-68-C-0236, Mar. 1969.
[18] R. M. White, "Surface elastic waves," *Proc. IEEE*, vol. 58, pp. 1238–1276, Aug. 1970.
[19] H. E. Rowe, *Signals and Noise in Communication Systems*. Princeton, N.J.: Van Nostrand, 1965.
[20] C. C. Tseng, "Frequency response of an interdigital transducer for excitation of surface elastic waves," *IEEE Trans. Electron Devices*, vol. ED-15, pp. 586–594, Aug. 1968.
[21] H. Engan, "Excitation of elastic surface waves by spatial harmonics of interdigital transducers," *IEEE Trans. Electron Devices*, vol. ED-16, pp. 1014–1017, Dec. 1969.
[22] C. C. Tseng and H. Engan, "Comments on 'Excitation of elastic surface waves by spatial harmonics of interdigital transducers,'" *IEEE Trans. Electron Devices* (Lett.), vol. ED-17, pp. 945–946, Oct. 1970.
[23] C. Atzeni, "Sensor number minimization in acoustic surface-wave matched filters," *IEEE Trans. Sonics Ultrason.*, vol. SU-18, pp. 193–201, Oct. 1971.
[24] P. H. Carr, "The generation and propagation of acoustic surface waves at microwaves frequencies," *IEEE Trans. Microwave Theory Tech. (Special Issue on Microwave Acoustics)*, vol. MTT-17, pp. 845–855, Nov. 1969.
[25] C. Atzeni, L. Masotti, and E. Teodori, "Acoustic surface-wave matched filters," *Alta Freq.*, vol. 40, pp. 506–512, June 1971.
[26] J. J. Kroszczyński, "Pulse compression by means of linear period modulation," *Proc. IEEE*, vol. 57, pp. 1260–1266, July 1969.
[27] C. Atzeni and L. Masotti, "Acoustic surface-wave processor for hyperbolic FM signals," *Electron. Lett.*, vol. 7, pp. 693–694, Nov. 1971.
[28] A. Papoulis, *The Fourier Integral and Its Applications*. New York: McGraw-Hill, 1962.
[29] C. Atzeni and L. Masotti, unpublished paper.
[30] R. C. Williamson, "Improved electrostatic probe for measurement of elastic surfaces waves," M.I.T. Lincoln Lab., Cambridge, Mass., Rep., 1971.
[31] R. W. Hamming, *Numerical Methods for Scientists and Engineers*. New York: McGraw-Hill, 1962.
[32] C. Lanczos, *Discourse on Fourier Series*. London, England: Oliver Boyd, 1966.
[33] C. Atzeni and L. Masotti, "Weighted interdigital transducers for smoothing of ripples in acoustic surface wave filters," *Electron. Lett.*, vol. 8, pp. 485–486, Sept. 1972.
[34] G. S. Kino and H. Matthews, "Signal processing in acoustic surface wave devices," *IEEE Spectrum*, vol. 8, pp. 22–35, Aug. 1971.

A Generalized Design Technique for Practical Distributed Reciprocal Ladder Networks

RALPH LEVY

***Abstract*—A generalized design approach is presented for ladder networks consisting of a cascade of constituent two-port networks connected by short lengths of transmission lines. The design is made possible by the derivation of simple equations which define the inverter impedance and associated reference planes of any passive lossless reciprocal two-port. This enables the general ladder network to be equated to a prototype network at a reference frequency. An example is given of the design of a coaxial low-pass filter where fringing capacitances are compensated automatically.**

Introduction

A DISTRIBUTED reciprocal ladder network illustrated in Fig. 1 is defined here as a cascade of reciprocal two-port subnetworks connected by means of transmission lines, which are usually all of approximately equal length and electrically short (between 0 and $3\lambda g/4$). The network is assumed to be lossless. The subnetworks may consist of simple primarily lumped elements such as inductive or capacitive irises or series gaps in a stripline, or distributed elements such as stubs or lengths of transmission line, or may be mixed lumped and distributed in character. Examples of such ladder networks are direct-coupled waveguide bandpass filters, coaxial low-pass filters, impedance transformers, or multielement directional couplers. The latter are four-ports, but if symmetrical, may be decomposed into two-port even- and odd-mode networks, and hence may be included in our category.

A large number of papers have been published on the design of individual ladder-network components, and a few have included a discussion of theoretical design features common to a wider class of structures. Examples of the latter include the use of lumped-element prototypes in the design of direct-coupled filters and the general concept of the impedance inverter by Cohn [1]. Another example is the introduction of the quarter-wave transformer as a prototype circuit for the design of many ladder networks by Young [2].

The result of a typical distributed network synthesis is an idealized component often consisting of a cascade of equal length (commensurate) lines, with or without commensurate stubs. In practice, the component will have junction and dis-

Manuscript received December 6, 1972; revised March 23, 1973.
The author is with Microwave Development Laboratories, Inc., Natick, Mass. 01760.